

ORIGINAL RESEARCH



# LTX-315-enabled, radiotherapy-boosted immunotherapeutic control of breast cancer by NK cells

Takahiro Yamazaki<sup>a</sup>, Erik Wennerberg<sup>a\*\*</sup>, Michal Hensler<sup>b</sup>, Aitziber Buqué<sup>a</sup>, Jeffrey Kraynak<sup>a</sup>, Jitka Fucikova<sup>b,c</sup>, Xi Kathy Zhou<sup>d</sup>, Baldur Sveinbjörnsson<sup>e,f,g</sup>, Øystein Rekdal<sup>b</sup>, Sandra Demaria<sup>a,h</sup>, and Lorenzo Galluzzi<sup>a,h,i</sup>

<sup>a</sup>Department of Radiation Oncology, Weill Cornell Medical College, New York, NY, USA; <sup>b</sup>Sotio, Prague, Czech Republic; <sup>c</sup>2nd Faculty of Medicine and University Hospital Motol, Department of Immunology, Charles University, Prague, Czech Republic; <sup>d</sup>Department of Population Health Sciences, Weill Cornell Medical College, New York, NY, USA; <sup>e</sup>Lytix Biopharma, Oslo, Norway; <sup>f</sup>Department of Medical Biology, University of Tromsø, Tromsø, Norway; <sup>g</sup>Childhood Cancer Research Unit, Department of Women and Children Health, Karolinska Institute, Stockholm, Sweden; <sup>h</sup>Sandra and Edward Meyer Cancer Center, New York, NY, USA; <sup>i</sup>Caryl and Israel Englander Institute for Precision Medicine, New York, NY, USA

## ABSTRACT

LTX-315 is a nonameric oncolytic peptide in early clinical development for the treatment of solid malignancies. Preclinical and clinical evidence indicates that the anticancer properties of LTX-315 originate not only from its ability to selectively kill cancer cells, but also from its capacity to promote tumor-targeting immune responses. Here, we investigated the therapeutic activity and immunological correlates of intratumoral LTX-315 administration in three syngeneic mouse models of breast carcinoma, with a focus on the identification of possible combinatorial partners. We found that breast cancer control by LTX-315 is accompanied by a reconfiguration of the immunological tumor microenvironment that supports the activation of anticancer immunity and can be boosted by radiation therapy. Mechanistically, depletion of natural killer (NK) cells compromised the capacity of LTX-315 to limit local and systemic disease progression in a mouse model of triple-negative breast cancer, and to extend the survival of mice bearing hormone-accelerated, carcinogen-driven endogenous mammary carcinomas. Altogether, our data suggest that LTX-315 controls breast cancer progression by engaging NK cell-dependent immunity.

## ARTICLE HISTORY

Received 10 July 2021  
Revised 27 July 2021  
Accepted 27 July 2021

## KEYWORDS

cDC1s; CTLA4; immune checkpoint inhibitors; MPA/DMBA-driven mammary carcinomas; PD-1; TS/A cells

## Introduction




Oncolytic peptides are emerging as attractive candidates for the development of novel anticancer regimens,<sup>1</sup> largely reflecting their ability to (1) target neoplastic cells based on relatively homogeneous membrane features, thus circumventing (at least some degree of) intratumoral heterogeneity,<sup>2</sup> and (2) mediate robust and multipronged immunostimulatory effects, hence favoring the initiation of tumor-targeting immune responses.<sup>3</sup> LTX-315 is a synthetic nonameric cationic peptide inspired from bovine lactotransferrin<sup>4</sup> that has demonstrated a particularly pronounced capacity to drive tumor-targeting immunity in preclinical cancer models.<sup>3</sup> Specifically, LTX-315 has been documented to kill cancer cells by engaging multiple modules of immunogenic cell death (ICD),<sup>5,6</sup> including the exposure of the endoplasmic reticulum (ER) chaperone calreticulin (CALR) on the cell surface, as well as the release of ATP, high mobility group box 1 (HMGB1), type I interferon (IFN), and mitochondrial components.<sup>7,8</sup> Moreover, LTX-315 has been shown to deplete the tumor microenvironment (TME) of immunosuppressive cells such as CD4<sup>+</sup>CD25<sup>+</sup>FOXP3<sup>+</sup> regulatory T (T<sub>REG</sub>) cells and myeloid-derived suppressor cells (MDSCs).<sup>9</sup> Consistent with this notion, LTX-315 synergized with immunogenic chemotherapeutics<sup>10</sup> or immune checkpoint inhibitors (ICIs)<sup>9</sup> in the control of mouse 4T1 mammary

carcinomas or MCA205 fibrosarcomas, respectively, established in immunocompetent syngeneic mice. Recent findings from a Phase I clinical trial enrolling patients with accessible, advanced solid tumors (NCT01986426) demonstrate that intratumoral LTX-315 has an acceptable safety profile, is clinically active, and induces changes in the immunological TME in support of anticancer immunity.<sup>11,12</sup>


Here, we investigated the ability of LTX-315 to cooperate with a panel of common immunostimulatory agents in mouse models of hormone receptor (HR)<sup>+</sup> and triple-negative breast cancer, focusing on the immunological correlates of activity and underlying mechanisms of action. Our findings suggest that LTX-315 controls breast cancer progression by immunotherapeutic effects that (at least in some settings) can be boosted by radiation therapy (RT), persist in the context of ICI-based immunotherapy, and rely on natural killer (NK) cells.

## Materials and methods

**Chemicals, cell lines and irradiation.** LTX-315 was provided by Lytix Biopharma. Unless otherwise specified, all other chemicals and lab reagents were obtained from Millipore Sigma. Mouse mammary adenocarcinoma TS/A cells were purchased from Millipore Sigma, while 4T1 cells were obtained from

**CONTACT** Lorenzo Galluzzi  [log3001@med.cornell.edu](mailto:log3001@med.cornell.edu)  Department of Radiation Oncology, Weill Cornell Medical College, New York, NY, USA; Sandra Demaria  [szd2005@med.cornell.edu](mailto:szd2005@med.cornell.edu)

**\*\*Current affiliation:** Division of Radiotherapy and Imaging, The Institute of Cancer Research, London, UK.

 Supplemental data for this article can be accessed on the [publisher's website](#)

© 2021 The Author(s). Published with license by Taylor & Francis Group, LLC.

This is an Open Access article distributed under the terms of the Creative Commons Attribution-NonCommercial License (<http://creativecommons.org/licenses/by-nc/4.0/>), which permits unrestricted non-commercial use, distribution, and reproduction in any medium, provided the original work is properly cited.

Dr. Fred Miller (Karmanos Cancer Center, Detroit, MI). Cells were maintained at 37°C under 5% CO<sub>2</sub>, in Dulbecco Modified Eagle Medium (DMEM) supplemented with 10% fetal bovine serum (FBS), 5 mM *L*-glutamine, 5 mM HEPES buffer, 50 μM β-mercaptoethanol 100 U mL<sup>-1</sup> penicillin sodium, 100 μg mL<sup>-1</sup> streptomycin sulfate and 50 μg mL<sup>-1</sup> gentamycin. Cell cultures were routinely authenticated by STR profiling (a service provided by IDEXX Bioresearch) and checked for *Mycoplasma* spp. contamination with the LookOut® Mycoplasma PCR Detection Kit. Irradiation of cells and mice was performed with a Small Animal Radiation Research Platform (SARRP, from Xstrahl).

**Flow cytometry – cell isolation and preparation of single-cell suspensions.** Mouse lungs, spleens, tumors, and tumor-draining lymph nodes (TDLNs) were excised immediately after sacrifice and weighed. Lungs and tumors were manually minced to small pieces using scalpels, followed by enzymatic and mechanical digestion using the Lung Dissociation Kit (#130-095-927, Miltenyi Biotec) and Tumor Dissociation Kit (130-096-730, Miltenyi Biotec), respectively, on a GentleMACS™ Octo Dissociator with Heaters (#130-096-427, Miltenyi Biotec) as per the manufacturer's instructions. Digested lungs and tumors were then passed through 70 μm strainers to remove undigested material and generate single-cell suspensions. Single-cell suspensions from spleens and TDLNs were generated by passing them through 70 μm strainers using the plunger of a syringe. Red blood cells (RBCs) were lysed by incubating cells in RBC Lysis Buffer (#420301, BioLegend) for 2 min and washing them twice in DMEM supplemented as above.

**Flow cytometry – staining.** Cell suspensions were incubated with antibodies specific for Fc receptor, IgG, low-affinity III (FCGR3, best known as CD16) and Fc receptor, IgG, low-affinity IIb (FCGR2B, best known as CD32), and then stained with eFluor 780 Fix Viability (#65-0865-14, Ebioscience) in PBS for 20 min at 4°C, followed by staining for surface markers with fluorochrome-conjugated antibodies (Table S1) for additional 20 min at 4°C. Cells were then fixed using the Cytofix/Cytoperm Kit (#554714, BD Biosciences) according to the manufacturer's instructions, followed by staining with antibodies specific for intracellular proteins (Table S1) for 20 min at 4°C. Samples were acquired on an LSRFortessa™ Flow Cytometer (BD Biosciences) or a MACSQuant Analyzer 10 (Miltenyi Biotec). FCS files were analyzed with FlowJo v. 10.2.6 (BD Biosciences). To correct for differences in auto-fluorescence between samples, mean fluorescence intensity (MFI) of each stained sample was subtracted of the MFI obtained in fluorescence minus one (FMO) conditions.

**Clonogenic assays.** Immediately after mouse euthanasia, lungs were perfused with PBS via the right cardiac ventricle and processed as detailed above to generate single cell suspensions. Cells were then washed twice in PBS and resuspended in 10 mL DMEM supplemented with 250 ng mL<sup>-1</sup> amphotericin B (#15290018, Thermo Fisher) and 60 μM 6-thioguanine, plated at a 1:9 dilution in 10 cm dishes, and allowed to form colonies for 7 d under standard culture conditions.<sup>13</sup> Colonies were fixed in 5 mL methanol at room temperature (RT), washed twice with distilled water, and stained with 5 ml methylene blue solution (0.03% v:v) for 5 min at RT. Excess

staining solution was discarded, colonies washed twice with distilled water, and dishes allowed to dry. Colonies were quantified by three blinded operators (T.Y., E.W., M.E.R.-R.).

**RNA sequencing.** Total RNA was isolated using the RNeasy Mini Kit (#74106, Qiagen). Following isolation, RNA integrity was checked using a 2100 Bioanalyzer (Agilent Technologies), and RNA concentration measured using a NanoDrop™ 2000 Spectrophotometers (Thermo Fisher). RNA library preparation and RNA sequencing were performed by the Genomics Core Laboratory of Weill Cornell Medicine. Messenger RNA was prepared using TruSeq Stranded mRNA Sample Library Preparation kit (Illumina) as per the manufacturer's instructions. Normalized cDNA libraries were pooled and sequenced on a NovaSeq 6000 sequencer (Illumina) with pair-end 50 cycles.

**RNA sequencing data mapping and analysis.** All RNA-seq data were mapped onto the mouse genome version mm10/GRCm38 using STAR 2.7.0c<sup>14</sup> as follows: STAR – readFilesIn \${FILE}.fastq.gz – genomeDir \$REF\_GENOME\_INDEX – runThreadN 8 – genomeLoad LoadAndRemove – limitBAMsortRAM 20000000000 – readFilesCommand zcat – outFilePrefix \${FILE}. – outSAMtype BAM SortedByCoordinate – outReadsUnmapped Fastx – outFilterMultimapNmax 99999 – outFilterMismatchNoverLmax 0.15 – outFilterMatchNminOverRead 0.66 – alignSJoverhangMin 10 – alignSJDBoverhangMin 10 – chimOutType Junctions – chimSegmentMin 10. Mapped reads were counted using program featureCounts,<sup>15</sup> as follows: featureCounts – a GENCODE.M15 – F \${FILE} – minOverlap 10 – fracOverlap 0.00 – s 2 – p – B – C – M – O – fraction – J – T 8 \${FILE}.bam. The GENCODE gene set (GENCODE M15) was used for the annotation. Differential expression analysis was performed using program suite DESeq2.<sup>16</sup> Unsupervised hierarchical clustering heatmaps were assembled for differentially expressed genes (DEGs) using the R package ComplexHeatmap<sup>17,18</sup> based on the Euclidean distance and Ward2 clustering method. Functional and enrichment analysis of DEGs was performed using the R package clusterProfiler.<sup>19</sup> The murine MCP-counter R package was used to estimate the abundance of tumor-infiltrating immune cell populations.<sup>20</sup>

**In vivo experiments.** Mice were housed in specific pathogen-free (SPF) conditions, and experimentation was aligned with the Guidelines for the Care and Use of Laboratory Animals guidelines and approved by the Institutional Animal Care and Use Committee (IACUC) of Weill Cornell Medical College (no. 2015-0028, 2018-0002). Double and triple TS/A tumors were obtained by subcutaneously injecting female 4–9-week-old BALB/cAnN mice (Taconic Bioscience), with 1 × 10<sup>5</sup> wildtype TS/A cells in one flank and 1 × 10<sup>5</sup> TS/A cells in the other flank only (double-lesion model) or in the other flank and in the back (triple-lesion model) 2 d later. 4T1 tumors were obtained by subcutaneously injecting female 6–9-week-old BALB/cAnN mice with 5 × 10<sup>4</sup> 4T1 cells. M/D-driven mammary tumors were established by subcutaneously implanting 6–9-week-old female C57BL/6J mice (Taconic Bioscience) with 50 mg slow-release (90 d) medroxyprogesterone acetate (MPA, M) pellets (Innovative Research of America) followed by oral gavage with 1 mg 7,12-dimethylbenz[a]anthracene (DMBA, D) in 200 μL corn oil

once a week on weeks 1, 2, 3, 5, 6, and 7 after pellet implantation.<sup>21</sup> Mice were then routinely assessed for the development of M/D-driven malignant lesions along the mammary lines. Mice bearing TS/A, 4T1, or M/D-driven mammary tumors were randomly allocated to treatment when surface tumor area calculated as the area of an ellipse ( $A = \text{longest diameter} \times \text{shortest diameter} \times \pi/4$ ) reached 12–30 mm<sup>2</sup> (d0). Primary treatments included (1) vehicle control: 50  $\mu$ L PBS delivered *i.t.* on d0, d1, d2; (2) focal RT: three fractions of 8 Gy each (total dose: 24 Gy; dose rate: 271 cGy/min) delivered to the primary tumor on d0, d1, d2; (3) low-dose LTX-315: 300  $\mu$ g LTX-315 delivered *i.t.* in 50  $\mu$ L vehicle on d0, d1, and d2; and (4) high-dose LTX-315: 300  $\mu$ g LTX-315 delivered *i.t.* in 50  $\mu$ L vehicle twice daily on d0, d1, and d2. CTLA4-targeting antibodies (9H10, from BioXCell) and PD-1-targeting antibodies (RMP1-14, from BioXCell) were delivered *i.p.* at 10 mg/kg as per the schedules illustrated in the figure set. Anti-asialo-GM1 antibodies (Poly21460, from BioLegend) and anti-NK1.1 antibodies (PK136, from BioXCell) were delivered *i.p.* at 12.5 mg/kg on d1 and then weekly until the end of the experiment. Mice were routinely assessed for the emergence of toxicity (troublesome breathing, weight loss, anorexia, hunched posture), growth of the primary (target) and secondary (abscopal) lesion(s) by a common caliper, as well as for the development and growth of secondary tumors (in the M/D-driven model).<sup>21</sup> TS/A-bearing mice were euthanized when cumulative tumor area reached 140–180 mm<sup>2</sup> surface area. 4T1-bearing mice were euthanized when primary tumor area reached 140–180 mm<sup>2</sup> or on d21 for the assessment of metastatic lung dissemination. Mice bearing M/D-driven tumors were euthanized when cumulative tumor area reached 180–200 mm<sup>2</sup>. Metastatic 4T1 cell dissemination to the lung surface was evaluated by two independent, blinded operators (T.Y., E. W.), using a DM-143 digital stereo microscope (Motic) upon lung fixation in 4% paraformaldehyde overnight, as previously described.<sup>22</sup> TS/A-bearing mice experiencing systemic disease eradication were subcutaneously rechallenged with  $1 \times 10^5$  wild-type TS/A cells to assess the development of immunological memory.

**Statistical analysis.** Data management, analysis, and graphing were performed with Prism v. 8.4 (GraphPad), Excel 265 ProPlus (Microsoft) or R v. 4.0.4. Statistical significance was assessed as follows: (1) tumor growth with a linear mixed-effects model plus simultaneous tests for general linear hypotheses; (2) relapse-free and overall survival curves with log-rank; (3) tumor rechallenge with Fisher exact test; (4) tumor infiltration by immune cells with Welch *t*-test; (5) correlations with the Spearman method; (6) differential gene expression with Wald test plus Benjamini–Hochberg correction; (7) gene set enrichment with clusterProfiler plus Benjamini–Hochberg correction; and (8) tumor area, clonogenic survival, metastatic dissemination, abundance of AH1<sup>+</sup> cells, and transcriptional signatures with Wilcoxon rank sum test. *p* values were considered significant when <0.05.

## Results

**Immunotherapeutic control of HR<sup>+</sup> TS/A mammary carcinomas by LTX-315.** We set to assess the immunotherapeutic

activity of LTX-315, alone or combined with RT, on TS/A mammary carcinomas, a commonly employed model of HR<sup>+</sup> breast cancer,<sup>23</sup> established subcutaneously in immunocompetent, syngeneic BALB/c mice. Since both LTX-315 and RT are administered locally, we opted for harnessing a double-lesion model that enables the assessment of systemic anticancer immunity.<sup>24</sup> To this aim, two slightly asynchronous TS/A tumors were established subcutaneously on either mouse flank, but while one of them would be allocated to treatment (primary tumor), the other one would remain untreated and serve as index lesion (secondary tumor) (Figure 1a). Three consecutive intratumoral injections of LTX-315 (300  $\mu$ g per dose) slightly reduced the growth of primary TS/A lesions, an effect that was considerably more pronounced when primary TS/A tumors were exposed to three consecutive RT doses of 8 Gy each (total dose: 24 Gy) (Figure 1b). RT and intratumoral LTX-315 administration exhibited some degree of cooperativity on the control of primary TS/A tumors (Figure 1b), but none of these regimens induced the control of distant, untreated TS/A lesions (Figure 1b). Conversely, combining RT with a cytotoxic T lymphocyte protein 4 (CTLA4)-targeting antibody (which *per se* has no effects in this model)<sup>25,26</sup> resulted not only in the complete regression of most irradiated TS/A tumors but also in a significant abscopal control of secondary lesions (Fig. S1).

To characterize the immunological circuitries driven by LTX-315 in the TME, primary and secondary TS/A lesions from the aforementioned experimental groups were collected 7 d after treatment initiation, dissociated and subjected to multiparametric flow cytometry. LTX-315 (and less so RT) caused an enrichment of CD45<sup>+</sup> cells in the TME of primary TS/A lesions, which was not further increased when these treatments were combined (Figure 1c and S2A). Conversely, RT + LTX-315 (but neither regimen alone) was associated with significant decrease in the relative proportion of tumor-infiltrating CD3<sup>+</sup> T lymphocytes (Figure 1c and S2A). No significant alterations were observed within the CD3<sup>+</sup> compartment of primary TS/A tumors in terms of CD4<sup>+</sup> vs. CD8<sup>+</sup> T cell distribution or CD4<sup>+</sup>FOXP3<sup>+</sup> T<sub>REG</sub> cell abundance (Figure 1c and S2A). RT (but not LTX-315) tended to reduce the fraction of CD4<sup>+</sup> (but not CD8<sup>+</sup>) T cells expressing the activation/exhaustion marker programmed cell death 1 (PDCD1, best known as PD-1), an effect that was antagonized in the context of LTX-315 + RT co-treatment (Figure 1c and S2A). The fraction of CD8<sup>+</sup> (but less so CD4<sup>+</sup>) T cells expressing the activation/exhaustion marker hepatitis A virus cellular receptor 2 (HAVCR2, best known as TIM-3) tended to increase in both LTX-315 – and RT-treated primary TS/A lesions, reaching statistical significance in tumors exposed to LTX-315 + RT (Figure 1c and S2A). Finally, CD8<sup>+</sup> T cells staining positively for the effector molecule interferon gamma (IFN $\gamma$ ) were significantly increased in TS/A lesions treated with LTX-315 + RT, as were CD4<sup>+</sup> T cells expressing the effector cytokine tumor necrosis factor (TFN) in irradiated tumors (Figure 1c and S2A). The relative abundance of CD11b<sup>+</sup> cells infiltrating primary TS/A lesions was also increased by LTX-315 + RT (Figure 1c and S2A). Moreover, LTX-315 seemed to drive an expansion of Ly6g<sup>+</sup> granulocytic cells, an effect that was antagonized when LTX-315 was combined with RT

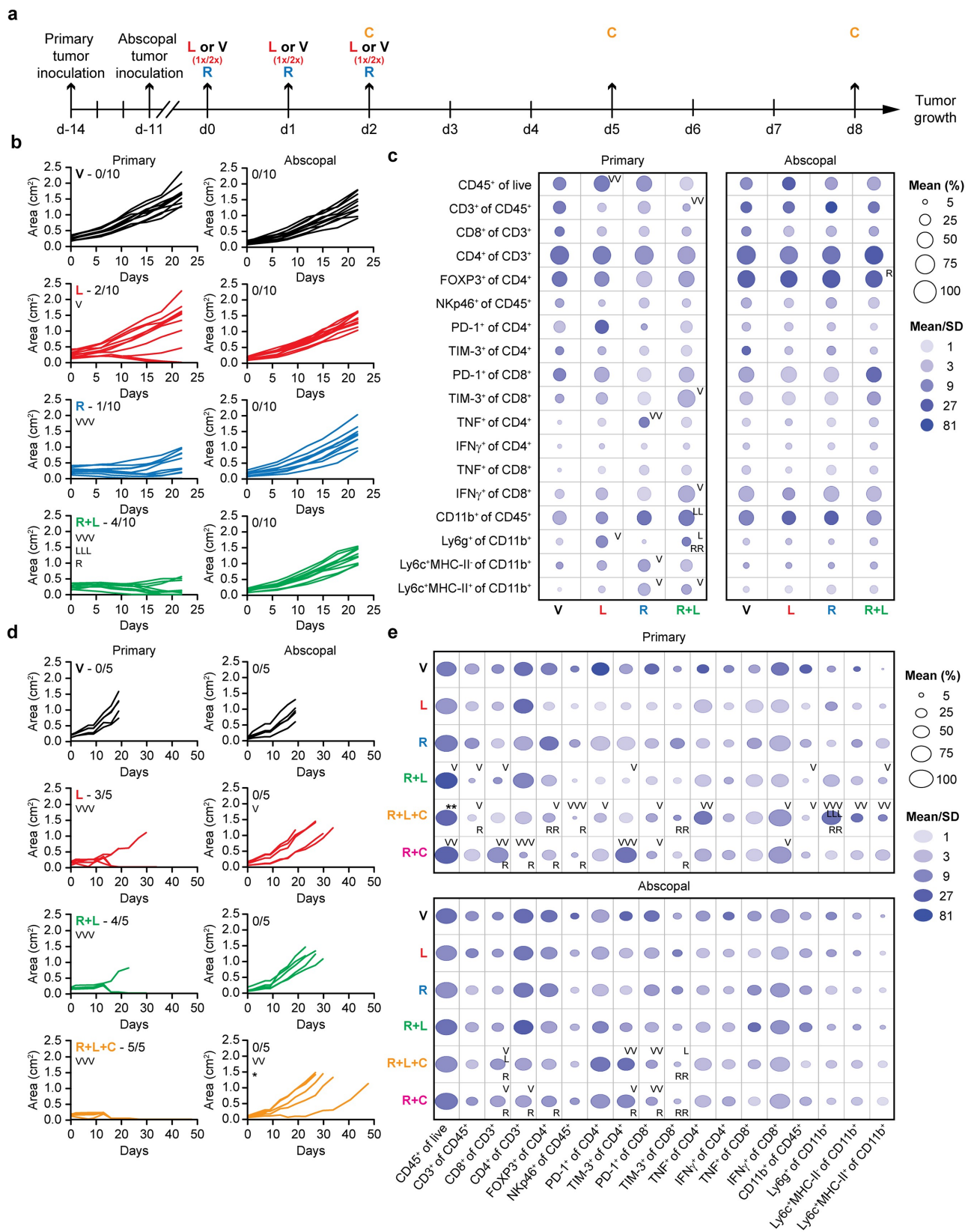


**Figure 1.** Immunotherapeutic control of HR<sup>+</sup> TS/A mammary carcinomas by LTX-315. (a) Experimental setup. C, CTLA4 blocker (9H10, 200  $\mu$ g, *i.p.*); L, LTX-315; (300  $\mu$ g, *i.t.*) R, radiation (8 Gy); V, vehicle. (b) Growth of primary and abscopal TS/A mammary carcinomas established in BALB/c mice that were subjected to the local (primary tumors only) or systemic treatments illustrated in (a) (one LTX-315 dose per day). Individual growth curves and incidence of tumor eradication are reported.  $V_p < .05$ ,  $VV_p < .01$ ,  $VVV_p < .001$  (linear mixed-effects model plus simultaneous tests for general linear hypotheses), as compared to the same lesion in V-treated mice;  $R_p < .05$ ,  $RR_p < .01$ ,  $RRR_p < .001$  (linear mixed-effects model plus simultaneous tests for general linear hypotheses), as compared to the same lesion in R-treated mice;  $L_p < .05$ ,  $LL_p < .01$ ,  $LLL_p < .001$  (linear mixed-effects model plus simultaneous tests for general linear hypotheses), as compared to the same lesion in L-treated mice. (c) Percentage of immune cells infiltrating primary and abscopal TS/A mammary carcinomas established in BALB/c mice that were subjected to the local (primary tumors only) or systemic treatments illustrated in (a) (one LTX-315 dose per day), and collected 7 d after treatment initiation. Means and means/SD are reported.  $n = 3$  mice per group.  $V_p < .05$ ,  $VV_p < .01$  (Welch *t*-test), as compared to the same lesion in V-treated mice;  $R_p < .05$ ,  $RR_p < .01$  (Welch *t*-test), as compared to the same lesion in R-treated mice;

<sup>L</sup>*p* < .05, <sup>LL</sup>*p* < .01 (Welch *t*-test), as compared to the same lesion in L-treated mice. See also Fig. S2.d. Growth of primary and abscopal TS/A mammary carcinomas established in BALB/c mice that were subjected to the local (primary tumors only) or systemic treatments illustrated in (a) (two LTX-315 doses per day). Individual growth curves and incidence of tumor eradication are reported. <sup>V</sup>*p* < .05, <sup>VV</sup>*p* < .01, <sup>VVV</sup>*p* < .001 (linear mixed-effects model plus simultaneous tests for general linear hypotheses), as compared to the same lesion in V-treated mice; <sup>#</sup>*p* < .05 (linear mixed-effects model plus simultaneous tests for general linear hypotheses), as compared to the same lesion in L + R-treated mice. (e) Percentage of immune cells infiltrating primary and abscopal TS/A mammary carcinomas established in BALB/c mice that were subjected to the local (primary tumors only) or systemic treatments illustrated in (a) (one LTX-315 dose per day), and collected 9 d after treatment initiation. Means and means/SD are reported. *n* = 3 mice per group. <sup>V</sup>*p* < .05, <sup>VV</sup>*p* < .01, <sup>VVV</sup>*p* < .001 (Welch *t*-test), as compared to the same lesion in V-treated mice; <sup>R</sup>*p* < .05, <sup>RR</sup>*p* < .01 (Welch *t*-test), as compared to the same lesion in R-treated mice; <sup>L</sup>*p* < .05, <sup>LL</sup>*p* < .001 (Welch *t*-test), as compared to the same lesion in L-treated mice; <sup>\*\*</sup>*p* < .01 (Welch *t*-test), as compared to the same lesion in R + C-treated mice. See also Fig. S3.

(Figure 1c and S2A). Among CD11b<sup>+</sup>Ly6g<sup>-</sup> myeloid cells, both Ly6c<sup>+</sup>MHC-II<sup>-</sup> and Ly6c<sup>+</sup>MHC-II<sup>+</sup> cells were expanded in irradiated TS/A tumors (Figure 1c and S2A). Importantly, virtually no variations were observed in the relative abundance of any of the aforementioned cell populations within secondary TS/A lesions (Figure 1c and S2B), correlating with the fact that none of these treatment regimens enabled abscopal responses (Figure 1b).

As LTX-315 administered intratumorally in three consecutive doses of 300 μg each had relatively limited effects on the growth of established TS/A tumors and could not drive abscopal responses when combined with RT, we increased LTX-315 daily dosage to 600 μg in total (delivered in two distinct intratumoral injections of 300 μg each) and combined this regimen with RT (8 Gy × 3), in the optional presence of a CTLA4 blocker (Figure 1a). At this dosage, LTX-315 delivered as a standalone agent had robust anticancer effects on primary TS/A lesions that globally manifested with a 60% disease eradication rate (Figure 1d). All combinatorial regimens (RT + LTX-315; RT + LTX-315 + CTLA4 blockage) were also associated with pronounced growth control and 80–100% eradication rate at the primary site (Figure 1d). However, abscopal tumor control was marginal in all cases, with the sole exception of the RT + LTX-315 + CTLA4 blockage regimen (Figure 1d). The relative contribution of LTX-315 to abscopal responses driven by RT + CTLA4 blockage (Fig. S1), however, remains to be elucidated.

The flow cytometry-assisted characterization of the immunological TME 9 d after treatment initiation revealed no significant changes in primary TS/A tumors receiving high-dose LTX-315 (Figure 1e and S3A). Conversely, lesions co-treated with LTX-315 and RT displayed an increased CD45<sup>+</sup> cell compartment that was characterized by a significant reduction in CD3<sup>+</sup> T cells, largely reflecting a decrease in the CD8<sup>+</sup> compartment (Figure 1e and S3A). T<sub>REG</sub> cells were decreased in TS/A tumors exposed to CTLA4 blockers (Figure 1e and S3A), as expected.<sup>27</sup> A significant reduction of PD-1<sup>+</sup>CD8<sup>+</sup> T cells coupled to an accumulation of TIM-3<sup>+</sup>CD4<sup>+</sup> T cells was seen in both primary and abscopal TS/A lesions from the RT + CTLA4 blockage treatment arm (Figure 1e and S3A, B). Moreover, CD8<sup>+</sup> T cells were enriched in the abscopal tumors of mice receiving RT + CTLA4 blockage or RT + LTX-315 + CTLA4 blockage (Figure 1e and S3A, B). Interestingly, RT alone tended to promote the accumulation of TIM-3<sup>+</sup>CD8<sup>+</sup> T cells in both irradiated and abscopal tumors, an effect that was quenched by CTLA4 blockage irrespective of LTX-315 (Figure 1e and S3A, B). In the primary lesions of mice treated with RT + LTX-315 + CTLA4 blockage, we observed a significant expansion of total Ly6g<sup>+</sup>CD11b<sup>+</sup> myeloid cells, as well as Ly6c<sup>+</sup>MHC-II<sup>-</sup> and Ly6c<sup>+</sup>MHC-II<sup>+</sup> cells, but no significant

changes in myeloid cells could be documented in abscopal tumors (Figure 1e and S3A, B). Along similar lines, CD3<sup>-</sup>NKp46<sup>+</sup> NK cells infiltrating primary TS/A lesions were reduced when RT was combined with CTLA4 blockage, an effect that persisted in the presence of LTX-315 (Figure 1e and S3A). Overall, early changes in the configuration of the immunological TME of abscopal TS/A lesions could only be documented in the context of systemic CTLA4 blockage, suggesting that intratumoral LTX-315 delivery (alone or combined with focal RT) does not affect the immune contexture of a synchronous tumor.

To test if sequence of administration may influence the ability of LTX-315 to cooperate with RT at the control of TS/A tumors, as observed for other immunomodulators,<sup>28–30</sup> we designed multiple combinatorial regimens differing in treatment schedule (Figure 2a), and assessed their efficacy in BALB/c mice bearing two slightly asynchronous TS/A lesions. Therapeutic efficacy at the primary (treated) site was remarkably similar irrespective of administration sequence, although the most prominent local control resulted from regimens involving late (as compared to early) CTLA4 blockage (Figure 2b). Conversely, the control of abscopal (untreated) tumors was maximal when LTX-315 and RT were delivered on the same days followed by CTLA4 blockage (Figure 2b). Indeed, such an effect was inhibited, at least to some degree, not only when the CTLA4-blocking antibody was delivered as first-line intervention, but also when LTX-315 and RT were administered sequentially (rather than simultaneously) prior to CTLA4 blockage (Figure 2b).

Intriguingly, the improved therapeutic activity of LTX-315 + RT followed by CTLA4 blockage was also observed when LTX-315 and RT were delivered to two different flank tumors and a tertiary dorsal tumor was used to assess systemic anticancer immunity (Figure 3a, b). In this context, 50% of the mice treated with LTX-315 to the primary tumor and RT to the secondary lesion experienced complete disease eradication (as compared to 33.33% for LTX-315 treatment to both flank tumors and 16.66% for RT to both flank tumors) (Figure 3c). Confirming the involvement of adaptive immunity, none of the mice that experienced long-term disease eradication upon treatment was permissive for the establishment of a novel TS/A tumor 60 d thereafter (Figure 3d).

Taken together, these findings suggest that LTX-315 and RT can be combined to generate robust anticancer responses that are systemically effective in combination with CTLA4 blockage in a tumor otherwise resistant to CTLA4 inhibitors.

**Immunotherapeutic control of triple-negative 4T1 mammary carcinomas by LTX-315.** We next assessed the immunotherapeutic effects of LTX-315 optionally combined with RT and ICIs in 4T1 mammary carcinomas, a model of metastatic,

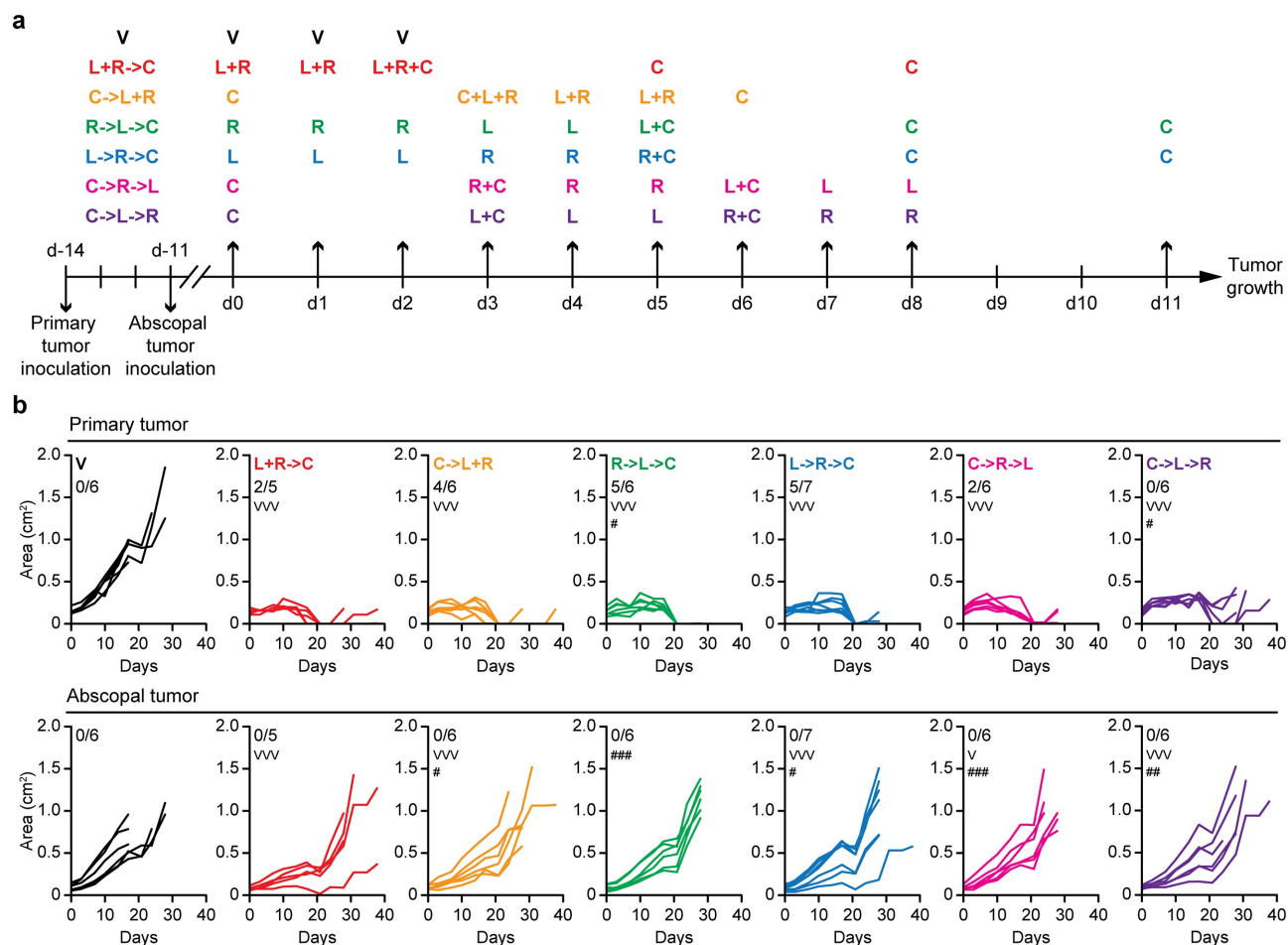


**Figure 2.** Impact of treatment schedule on the therapeutic efficacy of LTX-315 plus RT against HR<sup>+</sup> TS/A mammary carcinomas. (a) Experimental setup. C, CTLA4 blocker (9H10, 200  $\mu$ g, *i.p.*); L, LTX-315; (300  $\mu$ g, *i.t.*); R, radiation (8 Gy); V, vehicle. (b) Growth of primary and abscopal TS/A mammary carcinomas established in BALB/c mice that were subjected to the local (primary tumors only) or systemic treatments illustrated in (a). Individual growth curves and incidence of tumor eradication are reported. <sup>v</sup> $p < .05$ , <sup>vw</sup> $p < .001$  (linear mixed-effects model plus simultaneous tests for general linear hypotheses), as compared to the same lesion in V-treated mice; <sup>#</sup> $p < .05$ , <sup>##</sup> $p < .01$ , <sup>###</sup> $p < .001$  (linear mixed-effects model plus simultaneous tests for general linear hypotheses), as compared to the same lesion in mice receiving L + R followed by C.

poorly immunogenic (and hence ICI-insensitive) triple-negative breast cancer (TNBC) syngeneic to BALB/c mice.<sup>31</sup> In this setting (Figure 4a), three consecutive intratumoral injections of LTX-315 (300  $\mu$ g per dose) were virtually as efficient as three consecutive RT doses of 8 Gy each (total dose: 24 Gy) at controlling the progression of subcutaneous 4T1 tumors, an effect that was considerably more pronounced when the two treatment modalities were combined (Figure 4b), and correlated with a reduction in tumor-driven splenomegaly (a common systemic manifestation correlating with progressive disease) (Figure 4c), although it did not convert into superior survival (Figure 4d). While ICIs targeting CTLA4 or PD-1 had no effect on primary tumor growth in the 4T1 model, LTX-315 remained active in the context of ICI-based immunotherapy, both when employed alone and when combined with RT (Figure 4e and S4A–F). Consistent with local disease control, LTX-315 caused a considerable decrease in the number of macroscopic pulmonary metastases formed by progressing 4T1 tumors, an effect that was marginally improved by RT and persisted in the presence of PD-1 blockers (while RT and PD-1 blockers had no antimetastatic effects when employed as standalone interventions) (figure 4f). Similar results were

obtained by quantifying the number of malignant cells infiltrating the lung parenchyma by clonogenic assays (Figure 4g).

Unsupervised hierarchical clustering of RNAseq data suggests that intratumoral LTX-315 (300  $\mu$ g per dose in three consecutive days) only minimally alters the global transcriptional configuration of 4T1 tumors collected 12 d after treatment initiation (Figure 5a, b), potentially pointing to a transient transcriptional effect that does not persist over time. Conversely, RT as well as RT + CTLA4 blockage had more prominent effects on the transcriptional profile of 4T1 tumors collected at a similar time point, with some (but globally limited) alterations from the inclusion of LTX-315 in the treatment schedule (Figure 5a). Specifically, the immune-related transcriptome of 4T1 tumors collected 12 d after initiation of RT in three daily fractions of 8 Gy each was enriched in multiple genes linked to type I IFN signaling (e.g., *Ifit1*, *Ifit3*, *Ifit3b*), tumor infiltration by T cells (e.g., *Cd27*, *Cd3e*, *Cd3g*, *Cd8a*, *Cd8b1*) and NK cells (*Klr1*, *Klri2*, *Klre1*, *Klrc2*, *Klrc1*), as well as immune effector functions (e.g., *Il12rb2*, *Pdcd1*, *Havcr2*) (Figure 5b and Table S2). Intriguingly, as compared to RT alone, LTX-315 plus RT were associated with an immune-related transcriptional profile exhibiting an

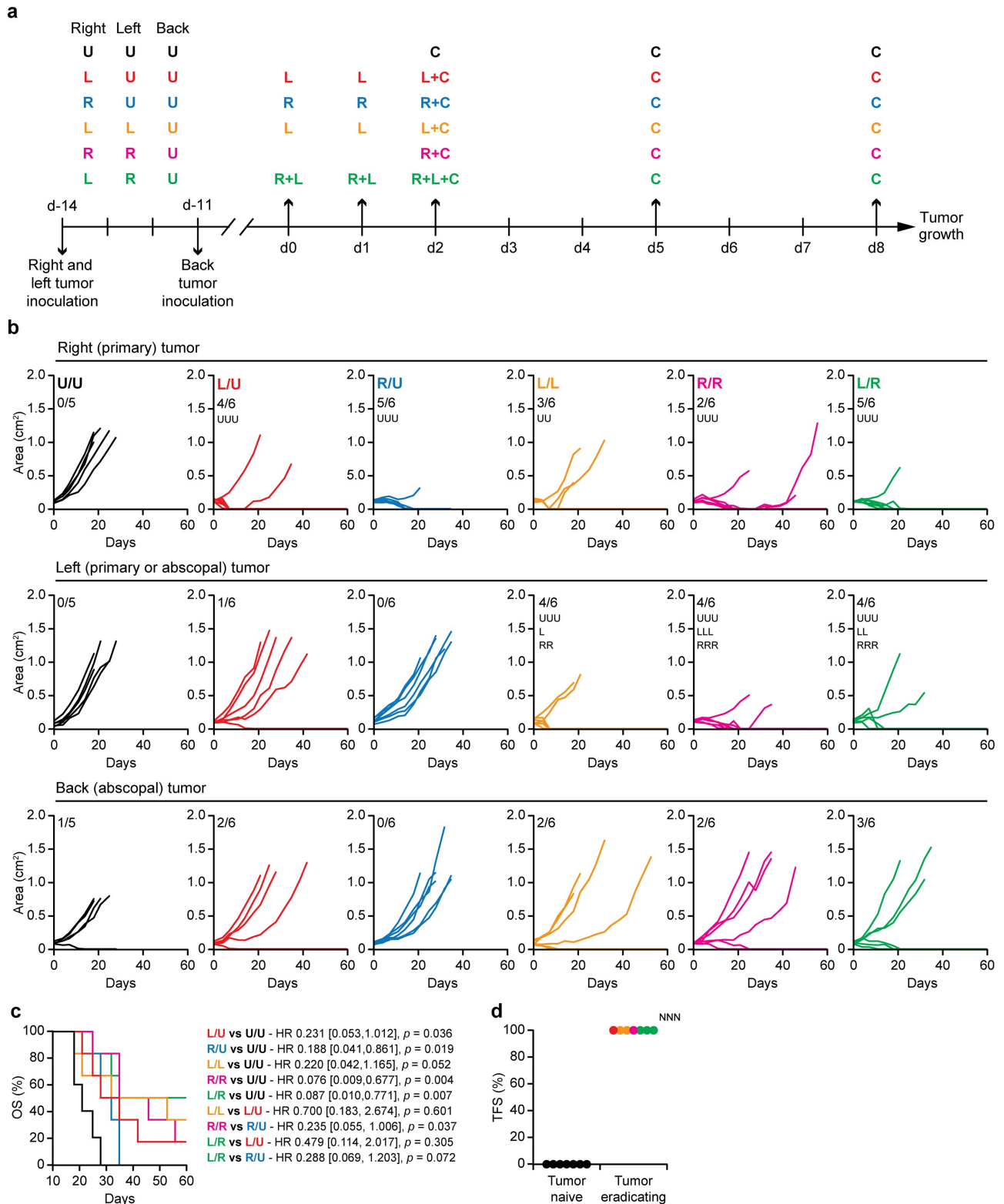


**Figure 3.** Impact of administration site on the therapeutic efficacy of LTX-315 plus RT against HR<sup>+</sup> TS/A mammary carcinomas. (a) Experimental setup. C, CTLA4 blocker (9H10, 200  $\mu$ g, *i.p.*); L, LTX-315; (300  $\mu$ g, *i.t.*) R, radiation (8 Gy); U, untreated. (b) Growth of primary and abscopal TS/A mammary carcinomas established in BALB/c mice that were subjected to the local (flank tumors only) or systemic treatments illustrated in (a). Individual growth curves and incidence of tumor eradication are reported.  $p_{UU} < .01$ ,  $p_{UUU} < .001$  (linear mixed-effects model plus simultaneous tests for general linear hypotheses), as compared to the same lesion in U/U mice;  $p_{RRR} < .001$  (linear mixed-effects model plus simultaneous tests for general linear hypotheses), as compared to the same lesion in R/U-treated mice;  $p_{LL} < .05$ ,  $p_{LLL} < .001$  (linear mixed-effects model plus simultaneous tests for general linear hypotheses), as compared to the same lesion in L/U mice; (c) Overall survival (OS) of BALB/c mice bearing triple TS/A lesions and treated as illustrated in (a). Hazard ratio (HR), 95% confidence interval and  $p$  values (log-rank) are reported. (d) Tumor-free survival (TFS) of tumor naïve BALB/c mice (black) or BALB/c mice bearing three distinct TS/A lesions that experience systemic disease eradication following treatment with LTX-315 to one lesion (red), LTX-315 to two lesions (yellow), RT to two lesions (pink) or LTX-315 to one lesion plus RT to two lesions (green) as illustrated in (a), upon rechallenge with a tumorigenic dose of TS/A cells *s.c.* Individual data points are reported.  $p_{NNN} < .001$  (Fisher exact test), as compared to tumor-naïve mice.

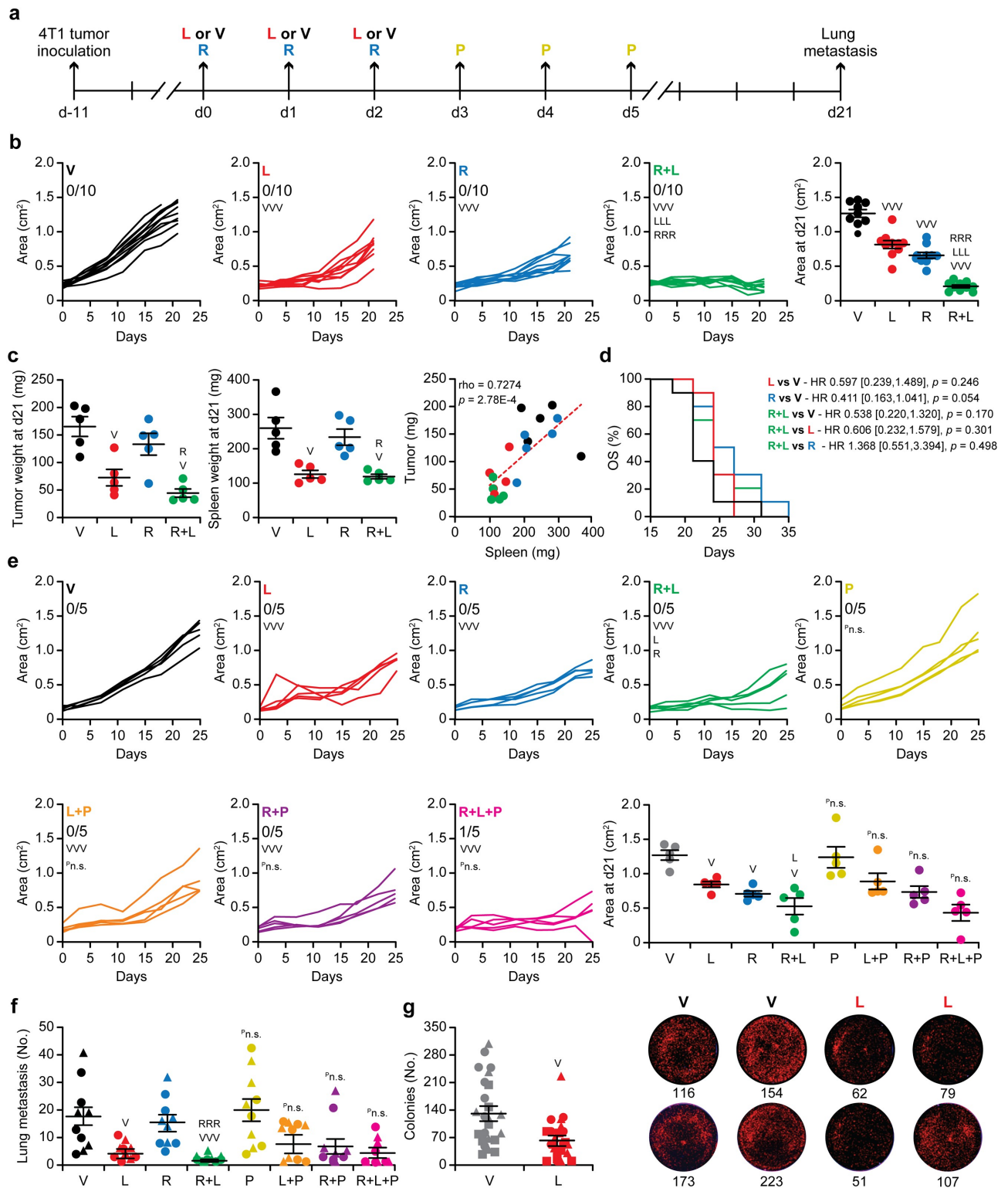


**Figure 4.** Therapeutic control of mouse 4T1 TNBCs by LTX-315. (a) Experimental setup. L, LTX-315; (300  $\mu$ g, *i.t.*); R, radiation (8 Gy); P, PD-1 blocker (RMP1-14, 200  $\mu$ g, *i.p.*); V, vehicle. (b) Growth of primary 4T1 mammary carcinomas established in BALB/c mice that were subjected to the local or systemic treatments illustrated in (a). Individual growth curves, incidence of tumor eradication as well as mean tumor area at d21  $\pm$  SEM and individual data points are reported. <sup>VVV</sup> $p < .001$  (linear mixed-effects model plus simultaneous tests for general linear hypotheses, Wilcoxon rank sum test for tumor area), as compared to V-treated mice; <sup>RRR</sup> $p < .001$  (linear mixed-effects model plus simultaneous tests for general linear hypotheses, Wilcoxon rank sum test for tumor area), as compared to R-treated mice; <sup>LLL</sup> $p < .001$  (linear mixed-effects model plus simultaneous tests for general linear hypotheses, Wilcoxon rank sum test for tumor area), as compared to L-treated mice. (c) Weight of (1) primary 4T1 mammary carcinomas established in BALB/c mice that were subjected to the local or systemic treatments illustrated in (a) upon collection at d21, and (2) spleens from the same mice. Results are means  $\pm$  SEM and individual data points. <sup>V</sup> $p < .05$  (Wilcoxon rank sum test), as compared to V-treated mice; <sup>R</sup> $p < .05$  (Wilcoxon rank sum test), as compared to R-treated mice. Linear regression curve, Spearman correlation coefficient ( $\rho$ ) and  $p$  value are reported. (d) Overall survival (OS) of BALB/c mice bearing 4T1 lesions and treated as illustrated in (a). Hazard ratio (HR), 95% confidence interval and  $p$  values (log-rank) are reported. (e) Growth of primary 4T1 mammary carcinomas established in BALB/c mice that were subjected to the local or systemic treatments illustrated in (a). Individual growth curves, incidence of tumor eradication as well as mean tumor area at d21  $\pm$  SEM and individual data points are reported. <sup>V</sup> $p < .05$ , <sup>VVV</sup> $p < .001$  (linear mixed-effects model plus simultaneous tests for general linear hypotheses, Wilcoxon rank sum test for tumor area), as compared to V-treated mice; <sup>R</sup> $p < .05$  (linear mixed-effects model plus



simultaneous tests for general linear hypotheses, Wilcoxon rank sum test for tumor area), as compared to R-treated mice;  $^Lp < .05$  (linear mixed-effects model plus simultaneous tests for general linear hypotheses, Wilcoxon rank sum test for tumor area), as compared to L-treated mice;  $^P$ n.s., not significant (linear mixed-effects model plus simultaneous tests for general linear hypotheses, Wilcoxon rank sum test for tumor area), as compared to mice receiving the same treatment in the absence of PD-1 blockage. (f) Number of macroscopic lung metastases in BALB/c mice bearing 4T1 mammary carcinomas that were subjected to the local or systemic treatments illustrated in (a). Results are means  $\pm$  SEM and individual data points from two independent operators (T.Y. and E.W.).  $^Vp < .05$ ,  $^{VVV}p < .001$  (linear mixed-effects model plus simultaneous tests for general linear hypotheses), as compared to V-treated mice;  $^{RRR}p < .001$  (linear mixed-effects model plus simultaneous tests for general linear hypotheses), as compared to R-treated mice;  $^P$ n.s., not significant (linear mixed-effects model plus simultaneous tests for general linear hypotheses), as compared to mice receiving the same treatment in the absence of PD-1 blockage. (g) Number of colony-forming cells isolated from the lung of 4T1-bearing BALB/c mice treated with vehicle or LTX-315 as illustrated in (a). Results are means  $\pm$  SEM and individual data points from two independent operators (T.Y. and E.W.) plus representative images from clonogenic assays.  $^Vp < .05$  (Welch test), as compared to V-treated mice.

underrepresentation of genes involved in cytotoxic effector functions (e.g., *Gzmg*, *Gzmd*, *Gzmf*, *Gzme*, *Prf1*) coupled to overrepresentation of transcripts involved in cytokine/chemokine signaling (e.g., *Il3ra*, *Il2*, *Il11ra2*, *Il11ra1*, *Il1rl2*, *Il1f5*, *Cxcl12*, *Ccl27b*, *Ccl27a*, *Tgfb2*, *Tgfb3l1*) and B cell infiltration (i.e., *Cd19*) (Figure 5b and Table S2). Several genes linked to cytokine/chemokine signaling (e.g., *Mx1*, *Il11ra2*, *Ccl9*, *Il11ra1*, *Cxcl3*, *Ccl6*, *Il1rl2*, *Ccl11*, *Il33*, *Cxcl5*, *Il13ra2*, *Il1f8*, *Il22ra1*, *Il1f5*, *Il20ra*, *Cxcl12*, *Il1f9*, *Ccl27a*, *Ccl27b*) and immunostimulation (*Tnfrsf18*, *Tnfsf11*) were also enriched in the immune-related transcriptome of 4T1 tumors responding to LTX-315 plus RT as compared to that of lesions responding to LTX-315 alone (Figure 5b and Table S2). Intriguingly, the addition of a CTLA4 blocker cause limited changes in the transcription of immune-related genes as compared to LTX-315 plus RT, largely restricted to a significant enrichment of *Cd14* (encoding a monocyte marker) as well as *Cxcl2* and *Ccr3* (both involved in cytokine/chemokine signaling) (Figure 5b and Table S2). When compared to the immunological transcriptomic profile of RT plus CTLA4 blockage, the immune-related transcriptional configuration of LTX-315 plus RT and CTLA4 blockage was associated with a significant underrepresentation of genes involved in cytotoxic effector functions (e.g., *Gzmn*, *Gzmd*, *Gzme*, *Gzmg*, *Gzmf*, *Gzmc*, *Gzmb*, *Prf1*) and cell death (e.g., *Casp3*, *Tnfrsf10b*, *Casp1*, *Casp8*) but also in immunosuppressive pathways (e.g., *Ido2*, *Tigit*, *Nt5e*), which was coupled with a reconfiguration of genes involved in cytokine/chemokine signaling (i.e., depletion of *Il12rb1*, *Cxcl1*, *Il23a*, *Il7*, *Tgfb1*, *Ilf3*, and enrichment of *Tnfrsf1a*, *Tgfb3l1*, *Il18*, *Il1rl2*, *Il17rc*, *Ccr3*, *Il20rb*, *Il1f6*) (Figure 5b and Table S2). As expected, the immune-related transcriptomic configuration of RT plus CTLA4 blockage exhibited a considerable enrichment in a variety of genes involved in cytokine/chemokine signaling (including type I IFN signaling) and immune effector functions (including cytotoxic effector functions), a number of changes that were only marginally altered in the presence of LTX-315 (Table S2). Gene set enrichment analysis (GSEA) based on Gene Ontology Biological Processes (Table S3), Reactome (Table S4), and Hallmarks (Figure 5c) signatures largely confirms these findings as it highlights various immune-unrelated gene sets to be further investigated.

The RNAseq-based deconvolution of the immunological TME of 4T1 tumors responding to LTX-315 (at the 300  $\mu$ g dose), RT or their combination by the MCP counter method<sup>32</sup> revealed that RT (but not LTX-315 delivery) is associated with an increase in gene signatures linked to T cells (and specifically CD8<sup>+</sup> T cells), which increases sub-significantly by LTX-315 co-administration (Fig. S5A). Combinatorial administration of LTX-315 plus RT and CTLA4 blockage was also associated

with an enrichment in gene signatures linked to T cells, as well as to an overrepresentation of genes involved in B cell and NK cell activity (Fig. S5A). Moreover, two genetic signatures of myeloid cells (encompassing *Nt5e*, *Entpd1*, *Cd38*, *Enpp1*, *Adora2a*, *Adora2b*, *Bst1*, *Cd26*, *Dpp4*, *P2ry2*, *P2rx7*, *Art2b*, *Art1*) and myeloid cell-dependent immunosuppression (encompassing *Tgfb1*, *Ido1*, *Cd38*, *Nt5e*, *Entpd1*, *Il10*) were both underrepresented in 4T1 tumors receiving LTX-315 + RT + CTLA4 blockage as compared to control tumors and lesions receiving RT only, an effect that could not be accounted for by CTLA4 inhibition *per se* (Fig. S5B). Conversely, little alterations were documented on a genetic signature of T-cell activation/exhaustion (encompassing *Ctla4*, *Pdcd1*, *Cd274*, *Vsiv*, *Lag3*, *Havcr2*, *Tigit*, *Klrc1*), with the exception of an RT-associated enrichment (Fig. S5B). Consistent with a decreased myeloid-dependent immunosuppression, 4T1 tumors receiving LTX-315 + RT + CTLA4 blockage were the only ones to be simultaneously enriched in transcripts coding for X-C motif chemokine ligand 1 (XCL1), C-C motif chemokine ligand 5 (CCL5) and fms related receptor tyrosine kinase 3 ligand (FLT3LG) (Fig. S5C), which are all involved in the establishment of a productive cross-talk between tumor-infiltrating cDC1s and NK cells.<sup>33,34</sup>

Multiparametric flow cytometry confirmed that the CD45<sup>+</sup> tumor microenvironment of LTX-315-treated 4T1 lesions (22 d after treatment initiation) is enriched of dendritic cells (DCs), notably cross-presenting XCR1<sup>+</sup> conventional type I DCs (cDC1s), as well as CD3<sup>+</sup> T cells and CD3<sup>-</sup>NKp46<sup>+</sup> NK cells (Figure 6a). However, neither the relative distribution of CD4<sup>+</sup> vs. CD8<sup>+</sup> T cells (Figure 6a), nor the expression levels of activation/exhaustion markers including CD69, tumor necrosis factor receptor superfamily, member 9 (TNFRSF9, best known as 4-1BB) and PD-1 on tumor-infiltrating T and NK cells (Figure 6b) were affected by treatment, with the exception of 4-1BB and PD-1 expression on NK cells from tumors exposed to LTX-315 plus RT (Figure 6b). At the splenic level, mice bearing LTX-315-treated 4T1 tumors manifested an enrichment in T lymphocytes and NK cells coupled to (1) a depletion in CD11b<sup>+</sup> myeloid cells, and (2) a repolarization of the myeloid compartment in favor of granulocytic MDSC depletion and enrichment of monocytic MDSCs and CD64<sup>+</sup> pro-inflammatory macrophages (especially in the context of RT) (Figure 6c). Of note, the lungs of BALB/c mice bearing LTX-315-treated 4T1 tumors also exhibited an accumulation of T and NK cells along with (1) a reduction in the myeloid cell compartment (Figure 6d), (2) an increased proportion of cDC1s over their CD11b<sup>+</sup>XCR1<sup>-</sup> type II counterparts (cDC2s) (Figure 6d), which negatively correlated with the overall abundance of myeloid cells (Figure 6e), and (3) an

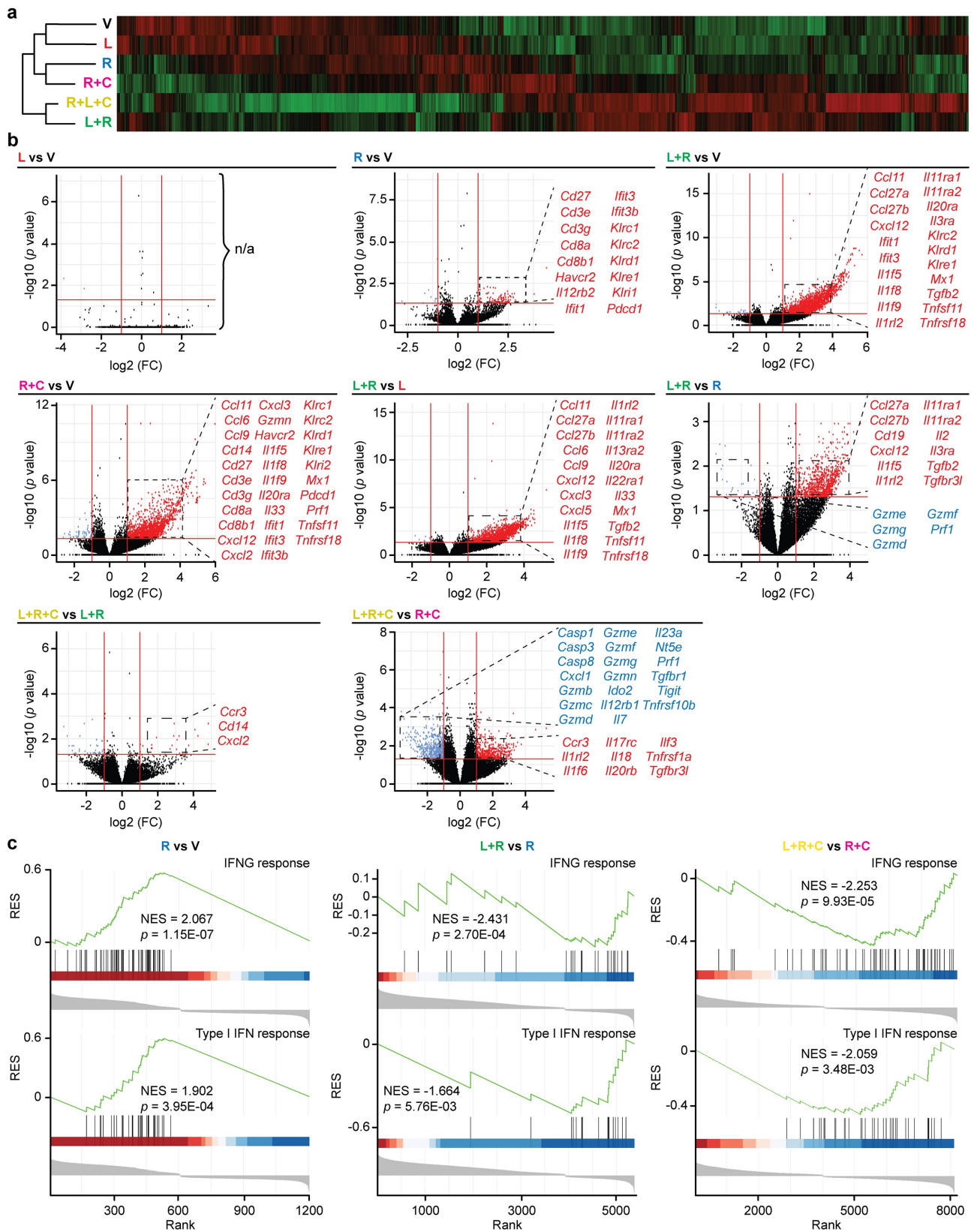


**Figure 4.** Transcriptional profile of mouse 4T1 TNBCs responding to LTX-315 and RT. (a) Unsupervised hierarchical clustering of the global transcriptional profile of mouse 4T1 TNBCs established in BALB/c mice subjected to the local or systemic treatments illustrated in Fig. S4a and collected 12 d after treatment initiation. See also Tables S2-4.b. Volcano plots for differentially expressed genes (DEGs) with log<sub>2</sub> fold change (FC) > 1 and adjusted p value (Wald test plus Benjamini–Hochberg correction) < 0.05. Immune-related genes of interest are indicated. See also Tables S2-4.c. Gene set enrichment analysis (GSEA) for Hallmarks signatures of type I interferon (IFN) and interferon gamma (IFNG) signaling. Normalized enrichment score (NES) and p values (clusterProfiler plus Benjamini–Hochberg correction) are reported. See also Table S2.

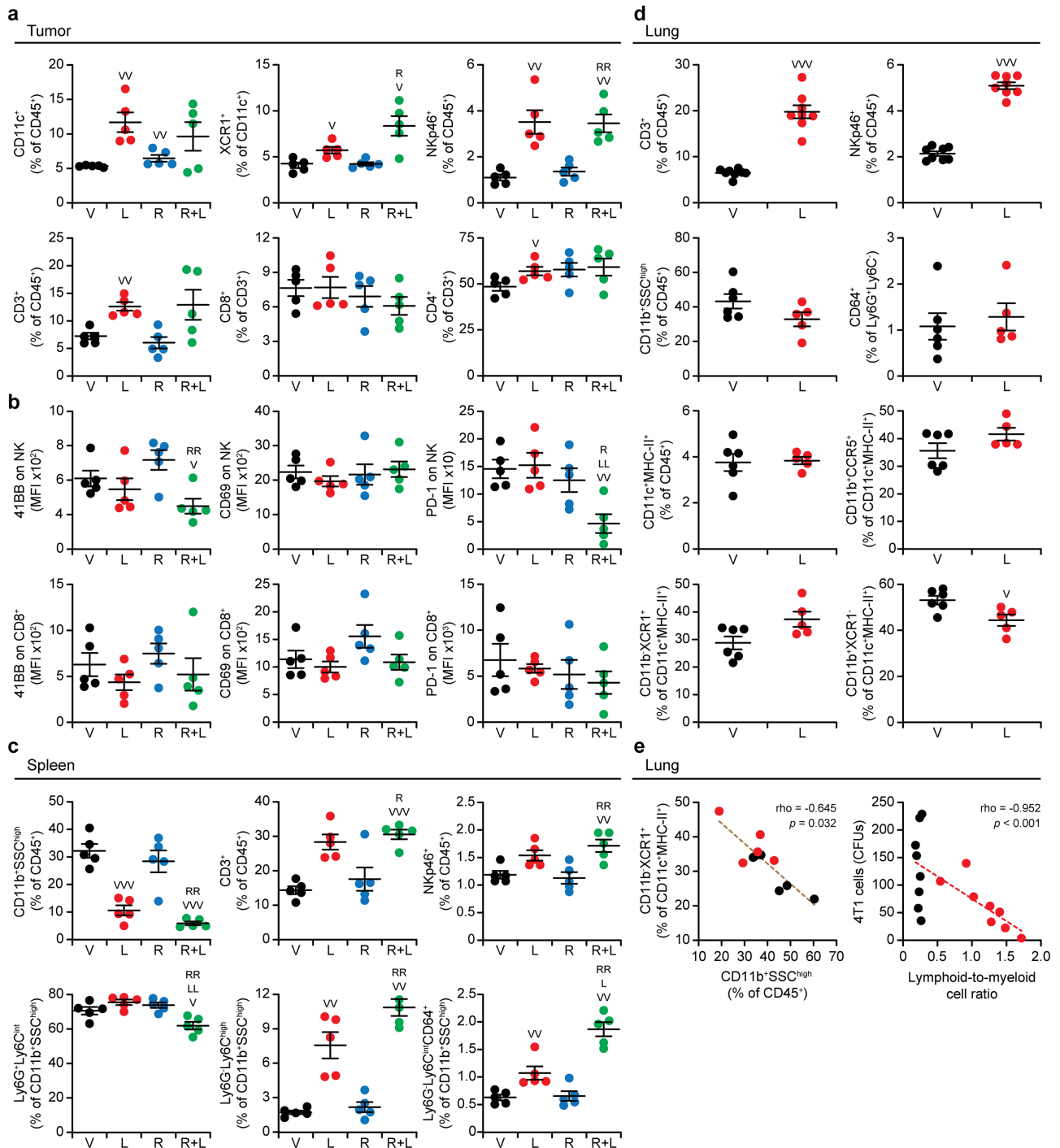


**Figure 6.** Immunological correlates of 4T1 TNBC control by LTX-315. (a–d) Percentage and/or surface phenotype of immune cells from the tumor (a, b), spleen (c) or lungs (d) of BALB/c mice bearing 4T1 TNBCs subjected to the local treatments illustrated in Fig. S4a in the absence of systemic PD-1 blockage, and collected 22 d after treatment initiation. Results are means  $\pm$  SEM and individual data points.  $^V p < .05$ ,  $^{VV} p < .01$ ,  $^{VVV} p < .001$  (Wilcoxon rank sum test), as compared to the same organ in V-treated mice;  $^R p < .05$ ,  $^{RR} p < .01$  (Wilcoxon rank sum test), as compared to the same organ in R-treated mice;  $^L p < .05$ ,  $^{LL} p < .01$  (Wilcoxon rank sum test), as compared to the same organ in L-treated mice. (e) Correlation between relative monocyte (Cd11b<sup>+</sup>SSC<sup>high</sup> cells) and cDC1 (CD11b<sup>+</sup>XCR1<sup>+</sup> cells) abundance or lymphoid-to-myeloid cell ratio (based on cell size and granularity, as determined by flow cytometry) and colony-forming 4T1 cells, as assessed in the lungs of 4T1-bearing mice 21 d after initiation of vehicle or LTX-315 treatment as illustrated in Fig. 4a in the absence of systemic PD-1 blockage. Linear regression curves, Spearman correlation coefficients ( $\rho$ ) and  $p$  values are reported. (f) Correlation between relative monocyte (Cd11b<sup>+</sup>SSC<sup>high</sup> cells) and cDC1 (CD11b<sup>+</sup>XCR1<sup>+</sup> cells) abundance in the lungs of 4T1-bearing mice 21 d after initiation of vehicle or LTX-315 treatment as illustrated in Fig. 4a in the absence of systemic PD-1 blockage. Linear regression curve, Spearman correlation coefficient ( $\rho$ ) and  $p$  value are reported.

inversion in the lymphoid-to-myeloid cell ratio, the magnitude of which inversely correlated with metastatic disease burden (Figure 6e). However, neither the tumor-draining lymph nodes nor the spleens of BALB/c mice bearing 4T1 lesions subjected to LTX-315 treatment exhibited an increase in CD8<sup>+</sup> T cells

specific for the immunodominant epitope AH1<sup>35</sup> (Fig. S4G), pointing to a limited engagement of T cell immunity in this model.

Taken together these data indicate that the ability of LTX-315 (alone or combined with RT) to control the primary

growth and metastatic dissemination of 4T1 tumors correlates with a repolarization of the local and systemic immune micro-environment in support of anticancer immunity, pointing to prominent a role for cDC1s and NK cells (but less so T lymphocytes).

#### Role of NK cells in the antineoplastic effects of LTX-315.

To dissect the relative mechanistic contribution of T lymphocytes and NK cells to the anticancer effects of LTX-315 we assessed LTX-315 dependent tumor control against 4T1 lesions established in *Rag1*<sup>-/-</sup> BALB/c mice, which lack T and B cells,<sup>36</sup> or in the context of antibody-dependent NK cell depletion. To our surprise, LTX-315 preserved its capacity to slow down the growth of primary 4T1 tumors in *Rag1*<sup>-/-</sup> mice (Figure 7a, b), while the depletion of NK cells with an anti-asialo GM1 antibody compromised the local therapeutic effects of LTX-315 (Figure 7b). Although in this set of experiments we observed a minimal (and statistically sub-significant) control of metastatic disease by LTX-315, the co-administration of NK cell-depleting antibodies (but less so the *Rag1*<sup>-/-</sup> genotype) fully compromised it (Figure 7c), suggesting that NK cells are also involved in systemic disease control by LTX-315.

To assess the validity of our findings in another preclinical model of breast cancer, we harnessed an endogenous mouse model of mammary carcinogenesis driven by a synthetic progestin, i.e., medroxyprogesterone acetate (MPA, M), and a polycyclic aromatic hydrocarbon, i.e., 7,12-dimethylbenz[a]anthracene (DMBA, D).<sup>21</sup> When established in immunocompetent C57BL/6 mice, M/D-driven mammary carcinomas recapitulate key genetic, transcriptional, immunological and treatment sensitivity features of human luminal B breast cancer,<sup>21,37</sup> in thus far representing a highly translational platform for the preclinical development of novel therapeutic regimens for HR<sup>+</sup> breast cancer. Intratumoral LTX-315 was highly effective at controlling the growth of M/D-driven tumors and extending the survival of M/D-driven tumor-bearing C57BL/6 mice (Figure 7d–f). Moreover, mice bearing M/D-driven mammary carcinomas treated with LTX-315 exhibited a longer relapse-free survival (RFS) as compared to M/D-driven tumor-bearing C57BL/6 mice that received no treatment (Figure 7g), which is indicative of enhanced immune control of secondary oncogenesis. Finally, NK cell depletion with an NK1.1-specific antibody limited local disease control (although sub-significantly) and survival extension (significantly) afforded by LTX-315 (Figure 7e, f), confirming a role for NK cells in the anticancer effects of LTX-315 against M/D-driven carcinomas.

Altogether, these findings suggest that LTX-315 engages an immune program that supports the NK cell-dependent control of various forms of breast cancer, at least in preclinical models of the disease.

## Discussion

Our data demonstrate that intratumoral LTX-315 administration mediates robust therapeutic effects in three distinct immunocompetent models of breast cancer, encompassing two transplantable models of ER<sup>+</sup> disease and TNBC syngeneic to BALB/c mice, and one endogenous model of luminal B breast

cancer established in C57BL/6 mice. In the transplantable models, local or systemic disease control by LTX-315 could be improved by RT delivered in three consecutive fractions of 8 Gy each, a dose/schedule that is known to enable the activation of adaptive tumor-targeting immune responses downstream of type I IFN secretion in the TME.<sup>38,39</sup> LTX-315 has also been shown to mediate multipronged immunostimulatory effects,<sup>3,40</sup> suggesting that at least part of the cooperativity between LTX-315 and RT would result from the improved activation of adaptive anticancer immunity.

Consistent with this notion, the TME of LTX-315-treated TS/A or 4T1 lesions exhibited multiple signs of repolarization in support of antigen-specific immune responses, especially in the context of LTX-315 + RT combinations. Moreover, TS/A-bearing BALB/c mice experiencing systemic disease eradication in the context of LTX-315 + RT co-treatment and CTLA4 inhibition were not permissive for the establishment of novel TS/A lesions, suggesting at least some degree of adaptive immunity. However, neither LTX-315 monotherapy nor LTX-315 + RT combos elicited the expansion of CD8<sup>+</sup> T cells specific for the immunodominant 4T1 antigen AH1. These latter findings suggested a limited mechanistic involvement of T-cell immunity in the anticancer effects of LTX-315, and rather pointed to the implication of other immune cell populations with (at least some) potential for immunological memory, such as NK cells.<sup>41,42</sup> Reinforcing this possibility, the local control of progressing 4T1 tumors by LTX-315 persisted in *Rag1*<sup>-/-</sup> mice, but was abolished by NK cell depletion with an anti-asialo GM1 antibody. Similar results were obtained when LTX-315 was employed against M/D-driven mammary carcinomas (which are under early natural immunosurveillance by NK cells),<sup>21,43</sup> in the context of NK cell depletion with an anti-NK1.1 antibody. Moreover, NK cell depletion with an anti-asialo GM1 antibody appeared to limit the control of metastatic tumor dissemination by LTX-315 in the 4T1 model, although in that specific set of experiments such control was quite suboptimal *a priori*. Taken together, these findings mechanistically point to NK cells as to central players in the ability of LTX-315 to control breast cancer progression, potentially in the context of memory-like responses. Thus, the ability of LTX-315 to control metastatic dissemination may be further boosted by interventions aimed at enhancing systemic NK cell functions such as (1) adoptive NK cell transfer,<sup>44</sup> (2) recombinant IL15 administration,<sup>45</sup> or (3) killer cell lectin like receptor C1 (KLRC1, best known as NKG2A) blockage.<sup>46</sup> That said, neither targeting asialo GM1 nor targeting NK1.1 enables the specific depletion of NK cells, as the former is also expressed by some other immune cell subsets including basophils,<sup>47</sup> and the latter is expressed by up to 50% of activated T cells,<sup>48</sup> suggesting that other cell populations may at least in part contribute to the effects we documented. Finally, our findings suggest that NK cells may play a role in the control of human breast cancer, which is in line with previous preclinical findings<sup>21,43</sup> and clinical data on the virtual insensitivity of the disease (especially, but not exclusively, in its luminal variants) to ICI-based immunotherapy.<sup>49–51</sup>

Of note, addition of LTX-315 to RT alone or combined with a CTLA4 blocker was associated with a decrease in the intratumoral abundance of transcripts coding for immune effector

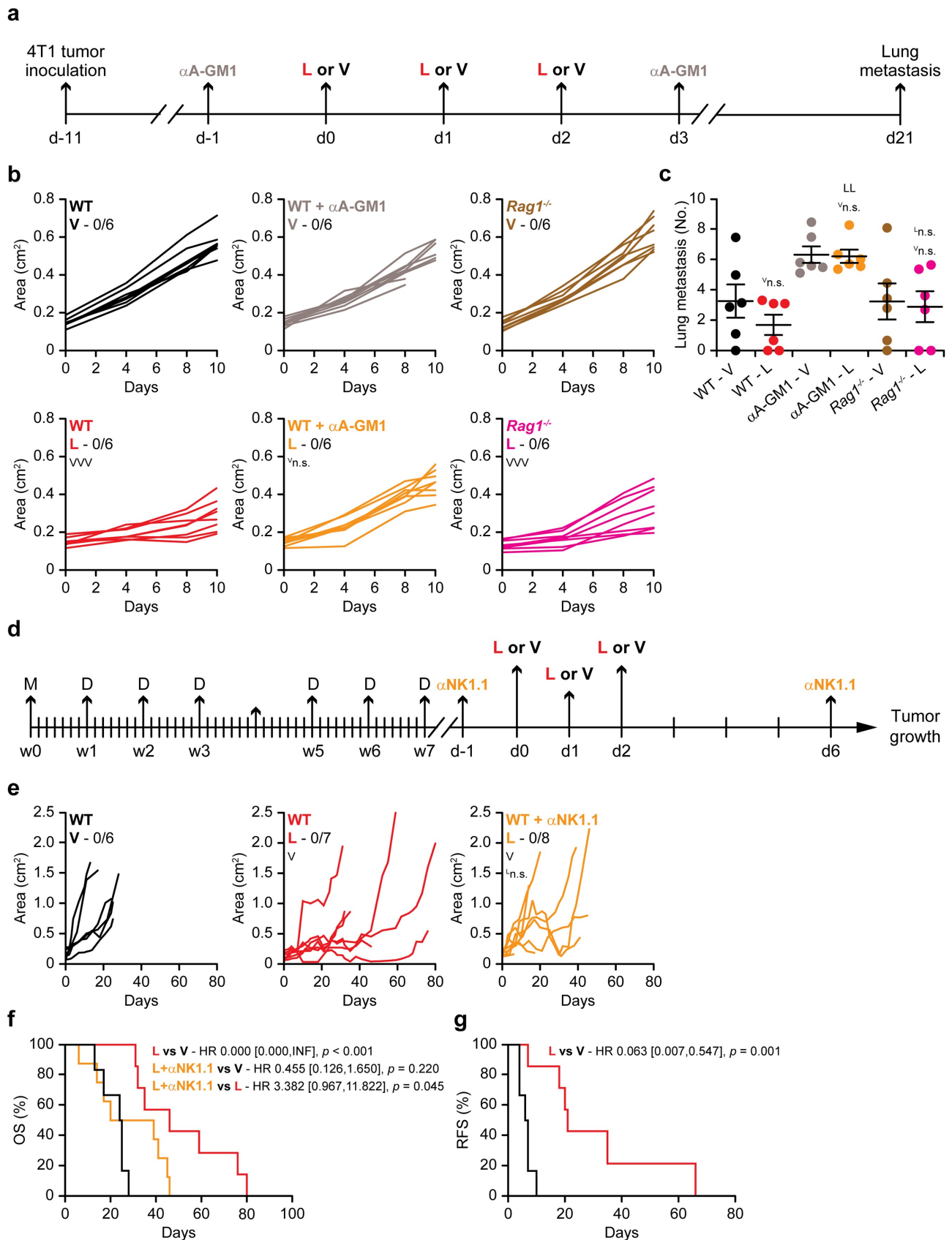


**Figure 7.** Impact of NK cells on breast cancer control by LTX-315. (a) Experimental setup for 4T1 tumors. αA-GM1, asialo GM1-targeting antibody; LTX-315; (300 μg, *i.t.*); V, vehicle. (b) Growth of primary 4T1 mammary carcinomas established in wild-type (WT) or *Rag1*<sup>-/-</sup> BALB/c mice that were subjected to the local or systemic treatments illustrated in (a). Individual growth curves and incidence of tumor eradication are reported. vns., not significant, wvw  $p < .001$  (linear mixed-effects model plus simultaneous tests for general linear hypotheses) as compared to V-treated mice of the same genotype and subjected to the same antibody-mediated depletion regimen. (c) Number of macroscopic lung metastases in WT or *Rag1*<sup>-/-</sup> BALB/c mice bearing 4T1 mammary carcinomas that were subjected to the local or systemic treatments illustrated in (a). Results are means ± SEM and individual data points from a single operator (E.W.). vns., not significant (Wilcoxon rank sum test), as compared to V-treated mice of the same genotype and subjected to the same antibody-mediated depletion regimen; n.s., not significant, <sup>L</sup> $p < .01$  (Wilcoxon rank sum

test), as compared to L-treated WT mice. (d) Experimental setup for M/D-driven tumors. aNK1.1, NK1.1-targeting antibody D, 7,12-dimethylbenz[a]anthracene; L, LTX-315; (300 µg, *i.t.*); M, medroxyprogesterone acetate; V, vehicle. (e-g) Tumor growth (e) overall survival (OS, f) and relapse-free survival (RFS, g) of WT C57BL/6 mice bearing primary endogenous M/D-driven mammary carcinomas that were subjected to the local or systemic treatments illustrated in (d). Individual growth curves and incidence of tumor eradication are reported.  $V_p < .05$  (linear mixed-effects model plus simultaneous tests for general linear hypotheses for tumor growth) as compared to V-treated mice; <sup>n.s.</sup>, not significant (linear mixed-effects model plus simultaneous tests for general linear hypotheses for tumor growth), as compared to L-treated mice. Hazard ratio (HR), 95% confidence interval and *p* values for OS (log-rank) are reported.

molecules including various members of the granzyme family and perforin 1 (PRF1), coupled with an enrichment for transcripts involved in interleukin 1 beta (IL1β, best known as IL-1β) or IL18 signaling. This observation raises the intriguing possibility that inflammasome activation by RT + LTX-315 may inhibit tumor-targeting immune responses, perhaps as a consequence of limited type I IFN signaling,<sup>52</sup> and hence may represent a target to further extend the efficacy of RT + LTX-315 combinations. Additional experiments harnessing inflammasome-incompetent models (e.g., *Aim2*<sup>-/-</sup> or *Nlrp3*<sup>-/-</sup> systems) or IL-1β antagonists (e.g., the FDA-approved drug anakinra)<sup>53</sup> are needed to formally assess this hypothesis.

Our experiments also investigated the optimal therapeutic setting for LTX-315 to cooperate with RT and/or ICIs, with specific focus on administration schedule and target lesion. While LTX-315 preserved its activity in ICI-insensitive models such as TS/A and 4T1 tumors, which recapitulate preliminary clinical data,<sup>54</sup> our findings suggest that using CTLA4 blockers as first-line therapeutic interventions may compromise, at least to some degree, the initiation of anticancer immune responses with systemic outreach by LTX-315 plus RT. These findings should be taken under attentive consideration in the design of clinical trial testing LTX-315 plus ICIs in patients. Moreover, our data support the notion that administering LTX-315 to one lesion and RT to a distant lesion may be superior to controlling both lesions with the same agent at eliciting the eradication of a third, untreated tumor. While these observations obviously cannot be extrapolated to the clinical settings as such, they raise the intriguing possibility that LTX-315 and RT may be combined in patients with both accessible (LTX-315 is administered intratumorally) and non-accessible (but eligible for irradiation) tumors. Further preclinical work is required to obtain additional insights into these potential avenues for clinical development.

Despite these and other unresolved questions, our work provides the first systematic characterization of intratumoral LTX-315 as a potential immunotherapeutic strategy to control breast cancer progression in partnership with RT.

## Acknowledgments

We are indebted to Dr. Fred Miller (Karmanos Cancer Center, Detroit, MI) for the kind gift of 4T1 cells, as well as to Dr. Karsten A. Pilonis (Weill Cornell Medicine, New York, NY) and Maria E. Rodriguez-Ruiz (University of Navarra, Pamplona, Spain) for help with clonogenic assays. This work has been sponsored by a research grant by Lytix Biopharma (Oslo, Norway) to S.D. and L.G.

## ORCID

Takahiro Yamazaki  <http://orcid.org/0000-0002-7420-4394>  
Øystein Rekdal  <http://orcid.org/0000-0001-5563-6709>

Sandra Demaria  <http://orcid.org/0000-0003-4426-0499>

## Author contributions

B.S., Ø.R., S.D. and L.G. conceived the project. T.Y., E.W. and A.B. performed experiments, analyzed data and prepared figures. J.K. provided technical assistance. M.H. and J.F. analyzed RNAseq data. X.K.Z. performed statistical assessments. S.D. and L.G. interpreted data and provided senior supervision to the project. L.G. wrote the manuscript with input from all authors. All authors approve the final version of the article and figures.

## Conflicts of interest

T.Y. has received salary support from Lytix Biopharma. M.H. and J.F. are full-time employees of Sotio. B.S. and Ø.R. are full-time employees and shareholders of Lytix Biopharma. S.D. has received research funding from Lytix Biopharma and Nanobiotix as well as consulting/advisory honoraria from Lytix Biopharma, EMD Serono, Ono Pharmaceutical, AstraZeneca, and Genentech. L.G. has received research funding from Lytix Biopharma and Phosplatin, as well as consulting/advisory honoraria from Boehringer Ingelheim, AstraZeneca, OmniSEQ, Onxeo, The Longevity Labs, Inzen, and the Luke Heller TECPR2 Foundation. All other authors have no conflicts of interest to disclose. As per standard operations at *Oncoimmunology*, LG has been excluded from the editorial evaluation of the present article.

## References

- Kepp O, Marabelle A, Zitvogel L, Kroemer G. Oncolysis without viruses - inducing systemic anticancer immune responses with local therapies. *Nat Rev Clin Oncol.* 2020;17(1):49–64. doi:10.1038/s41571-019-0272-7.
- Vitale I, Shema E, Loi S, Galluzzi L. Intratumoral heterogeneity in cancer progression and response to immunotherapy. *Nat Med.* 2021;27(2):212–224. doi:10.1038/s41591-021-01233-9.
- Vitale I, Yamazaki T, Wennerberg E, Sveinbjørnsson B, Rekdal Ø, Demaria S, Galluzzi L. Targeting cancer heterogeneity with immune responses driven by oncolytic peptides. *Trends Cancer.* 2021;7(6):557–572. doi:10.1016/j.trecan.2020.12.012.
- Camilio KA, Berge G, Ravuri CS, Rekdal O, Sveinbjørnsson B. Complete regression and systemic protective immune responses obtained in B16 melanomas after treatment with LTX-315. *Cancer Immunol Immunother.* 2014;63(6):601–613. doi:10.1007/s00262-014-1540-0.
- Galluzzi L, Vitale I, Warren S, Adjemian S, Agostinis P, Martinez AB, Chan TA, Coukos G, Demaria S, Deutsch E, et al. Consensus guidelines for the definition, detection and interpretation of immunogenic cell death. *J Immunother Cancer.* 2020;8(1):e000337.
- Sprooten J, Garg AD. Type I interferons and endoplasmic reticulum stress in health and disease. *Int Rev Cell Mol Biol.* 2020;350:63–118.
- Eike LM, Yang N, Rekdal Ø, Sveinbjørnsson B. The oncolytic peptide LTX-315 induces cell death and DAMP release by mitochondria distortion in human melanoma cells. *Oncotarget.* 2015;6(33):34910–34923. doi:10.18632/oncotarget.5308.
- Zhou H, Forveille S, Sauvat A, Yamazaki T, Senovilla L, Ma Y, Liu P, Yang H, Bezu L, Müller K, et al. The oncolytic peptide LTX-315 triggers immunogenic cell death. *Cell Death Dis.* 2016;7(3):e2134. doi:10.1038/cddis.2016.47.

9. Yamazaki T, Pitt JM, Vétizou M, Marabelle A, Flores C, Rekdal Ø, Kroemer G, Zitvogel L. The oncolytic peptide LTX-315 overcomes resistance of cancers to immunotherapy with CTLA4 checkpoint blockade. *Cell Death Differ.* 2016;23(6):1004–1015. doi:10.1038/cdd.2016.35.
10. Camilio KA, Wang MY, Mauseth B, Waagene S, Kvalheim G, Ø R, Sveinbjørnsson B, Mælandsmo GM. Combining the oncolytic peptide LTX-315 with doxorubicin demonstrates therapeutic potential in a triple-negative breast cancer model. *Breast Cancer Res.* 2019;21:9. doi:10.1186/s13058-018-1092-x.
11. Jebsen NL, Apelseh TO, Haugland HK, Rekdal Ø, Patel H, Gjertsen BT, Jøssang DE. Enhanced T-lymphocyte infiltration in a desmoid tumor of the thoracic wall in a young woman treated with intratumoral injections of the oncolytic peptide LTX-315: a case report. *J Med Case Rep.* 2019;13(1):177. doi:10.1186/s13256-019-2088-6.
12. Spicer J, Marabelle A, Baurain JF, Jebsen NL, Jøssang DE, Awada A, Kristeleit R, Loirat D, Lazaridis G, Jungels C, et al. Safety, antitumor activity, and T-cell responses in a dose-ranging phase I trial of the oncolytic peptide LTX-315 in patients with solid tumors. *Clin Cancer Res.* 2021;27(10):2755–2763. doi:10.1158/1078-0432.CCR-20-3435.
13. Aslakson CJ, Miller FR. Selective events in the metastatic process defined by analysis of the sequential dissemination of subpopulations of a mouse mammary tumor. *Cancer Res.* 1992;52:1399–1405.
14. Dobin A, Davis CA, Schlesinger F, Drenkow J, Zaleski C, Jha S, Batut P, Chaisson M, Gingeras TR. STAR: ultrafast universal RNA-seq aligner. *Bioinformatics.* 2013;29(1):15–21. doi:10.1093/bioinformatics/bts635.
15. Liao Y, Smyth GK, Shi W. featureCounts: an efficient general purpose program for assigning sequence reads to genomic features. *Bioinformatics.* 2014;30(7):923–930. doi:10.1093/bioinformatics/btt656.
16. Love MI, Huber W, Anders S. Moderated estimation of fold change and dispersion for RNA-seq data with DESeq2. *Genome Biol.* 2014;15(12):550. doi:10.1186/s13059-014-0550-8.
17. Gu Z, Eils R, Schlesner M. Complex heatmaps reveal patterns and correlations in multidimensional genomic data. *Bioinformatics.* 2016;32(18):2847–2849. doi:10.1093/bioinformatics/btw313.
18. Hensler M, Kasikova L, Fiser K, Rakova J, Skapa P, Laco J, Lanickova T, Pecen L, Truxova I, Vosahlikova S, et al. M2-like macrophages dictate clinically relevant immunosuppression in metastatic ovarian cancer. *J Immunother Cancer.* 2020;8(2):e000979.
19. Yu G, Wang LG, Han Y, He QY. clusterProfiler: an R package for comparing biological themes among gene clusters. *OmicS.* 2012;16(5):284–287. doi:10.1089/omi.2011.0118.
20. Petitprez F, Levy S, Sun CM, Meylan M, Linhard C, Becht E, Elarouci N, Tavel D, Roumenina LT, Ayadi M, et al. The murine microenvironment cell population counter method to estimate abundance of tissue-infiltrating immune and stromal cell populations in murine samples using gene expression. *Genome Med.* 2020;12(1):86. doi:10.1186/s13073-020-00783-w.
21. Buqué A, Bloy N, Perez-Lanzón M, Iribarren K, Humeau J, Pol JG, Levesque S, Mondragon L, Yamazaki T, Sato A, et al. Immunoprophylactic and immunotherapeutic control of hormone receptor-positive breast cancer. *Nat Commun.* 2020;11(1):3819. doi:10.1038/s41467-020-17644-0.
22. Pilonis KA, Hensler M, Daviaud C, Kraynak J, Fucikova J, Galluzzi L, Demaria S, Formenti SC. Converging focal radiation and immunotherapy in a preclinical model of triple negative breast cancer: contribution of VISTA blockade. *Oncoimmunology.* 2020;9(1):1830524. doi:10.1080/2162402X.2020.1830524.
23. De Giovanni C, Nicoletti G, Landuzzi L, Palladini A, Lollini PL, Nanni P. Bioprofiling TS/A murine mammary cancer for a functional precision experimental model. *Cancers (Basel).* 2019;11(12):1889. doi:10.3390/cancers11121889.
24. Rodriguez-Ruiz ME, Buqué A, Hensler M, Chen J, Bloy N, Petroni G, Sato A, Yamazaki T, Fucikova J, Galluzzi L. Apoptotic caspases inhibit abscopal responses to radiation and identify a new prognostic biomarker for breast cancer patients. *Oncoimmunology.* 2019;8(11):e1655964. doi:10.1080/2162402X.2019.1655964.
25. Dewan MZ, Galloway AE, Kawashima N, Dewyngaert JK, Babb JS, Formenti SC, Demaria S. Fractionated but not single-dose radiotherapy induces an immune-mediated abscopal effect when combined with anti-CTLA-4 antibody. *Clin Cancer Res.* 2009;15(17):5379–5388. doi:10.1158/1078-0432.CCR-09-0265.
26. Yamazaki T, Kirchmair A, Sato A, Buqué A, Rybstein M, Petroni G, Bloy N, Finotello F, Stafford L, Navarro Manzano E, et al. Mitochondrial DNA drives abscopal responses to radiation that are inhibited by autophagy. *Nat Immunol.* 2020;21(10):1160–1171. doi:10.1038/s41590-020-0751-0.
27. Simpson TR, Li F, Montalvo-Ortiz W, Sepulveda MA, Bergerhoff K, Arce F, Roddie C, Henry JY, Yagita H, Wolchok JD, et al. Fc-dependent depletion of tumor-infiltrating regulatory T cells co-defines the efficacy of anti-CTLA-4 therapy against melanoma. *J Exp Med.* 2013;210(9):1695–1710. doi:10.1084/jem.20130579.
28. Petroni G, Buqué A, Yamazaki T, Bloy N, Liberto MD, Chen-Kiang S, Formenti SC, Galluzzi L. Radiotherapy delivered before CDK4/6 inhibitors mediates superior therapeutic effects in ER + breast cancer. *Clin Cancer Res.* 2021;27(7):1855–1863. doi:10.1158/1078-0432.CCR-20-3871.
29. Petroni G, Galluzzi L. Impact of treatment schedule on the efficacy of cytostatic and immunostimulatory agents. *Oncoimmunology.* 2021;10(1):1889101. doi:10.1080/2162402X.2021.1889101.
30. Wei J, Montalvo-Ortiz W, Yu L, Krasco A, Ebstein S, Cortez C, Lowy I, Murphy AJ, Sleeman MA, Skokos D. Sequence of alphaPD-1 relative to local tumor irradiation determines the induction of abscopal antitumor immune responses. *Sci Immunol.* 2021;6(58):eabg0117.
31. Mosely SI, Prime JE, Sainson RC, Koopmann JO, Wang DY, Greenawalt DM, Ahdesmaki MJ, Leyland R, Mullins S, Pacelli L, et al. Rational selection of syngeneic preclinical tumor models for immunotherapeutic drug discovery. *Cancer Immunol Res.* 2017;5(1):29–41. doi:10.1158/2326-6066.CIR-16-0114.
32. Becht E, Giraldo NA, Lacroix L, Buttard B, Elarouci N, Petitprez F, Selves J, Laurent-Puig P, Sautès-Fridman C, Fridman WH, et al. Estimating the population abundance of tissue-infiltrating immune and stromal cell populations using gene expression. *Genome Biol.* 2016;17(1):218. doi:10.1186/s13059-016-1070-5.
33. Böttcher JP, Bonavita E, Chakravarty P, Blees H, Cabeza-Caberizo M, Sammicheli S, Rogers NC, Sahai E, Zelenay S, Reis e Sousa C. NK Cells Stimulate Recruitment of cDC1 into the Tumor Microenvironment Promoting Cancer Immune Control Cell. 2018;172:1022–37.e14.
34. Bötter J, Zahan T, van Slooten R, Schreiber G, De Vries IJM, Flórez-Grau G. Harnessing the cDC1-NK cross-talk in the tumor microenvironment to battle cancer. *Front Immunol.* 2020;11:631713. doi:10.3389/fimmu.2020.631713.
35. Aes TL, Vandenabeele P. The intrinsic immunogenic properties of cancer cell lines, immunogenic cell death, and how these influence host antitumor immune responses. *Cell Death Differ.* 2021;28(3):843–860. doi:10.1038/s41418-020-00658-y.
36. Falk I, Potocnik AJ, Barthlott T, Levelt CN, Eichmann K. Immature T cells in peripheral lymphoid organs of recombinase-activating gene-1/-2-deficient mice. Thymus Dependence and Responsiveness to anti-CD3 Epsilon Antibody *J Immunol.* 1996;156:1362–1368.
37. Abba MC, Zhong Y, Lee J, Kil H, Lu Y, Takata Y, Simper MS, Gaddis S, Shen J, Aldaz CM. DMBA induced mouse mammary tumors display high incidence of activating Pik3caH1047 and loss of function Pten mutations. *Oncotarget.* 2016;7(39):64289–64299. doi:10.18632/oncotarget.11733.
38. Vanpouille-Box C, Alard A, Aryankalayil MJ, Sarfraz Y, Diamond JM, Schneider RJ, Inghirami G, Coleman CN, Formenti SC, Demaria S. DNA exonuclease Trex1 regulates

- radiotherapy-induced tumour immunogenicity. *Nat Commun.* 2017;8(1):15618. doi:10.1038/ncomms15618.
39. Rodriguez-Ruiz ME, Vitale I, Harrington KJ, Melero I, Galluzzi L. Immunological impact of cell death signaling driven by radiation on the tumor microenvironment. *Nat Immunol.* 2020;21(2):120–134. doi:10.1038/s41590-019-0561-4.
  40. Rao S, Gharib K, Han A. Cancer immunosurveillance by T cells. *Int Rev Cell Mol Biol.* 2019;342:149–173.
  41. von Andrian UH. NK cell memory: discovery of a mystery. *Nat Immunol.* 2021;22(6):669–671. doi:10.1038/s41590-021-00890-9.
  42. Gang M, Wong P, Berrien-Elliott MM, Fehniger TA. Memory-like natural killer cells for cancer immunotherapy. *Semin Hematol.* 2020;57:185–193.
  43. Buque A, Bloy N, Petroni G, Kroemer G, Galluzzi L. NK cells beat T cells at early breast cancer control. *Oncoimmunology.* 2020;9(1):1806010. doi:10.1080/2162402X.2020.1806010.
  44. Myers JA, Miller JS. Exploring the NK cell platform for cancer immunotherapy. *Nat Rev Clin Oncol.* 2021;18(2):85–100. doi:10.1038/s41571-020-0426-7.
  45. Pilonis KA, Charpentier M, Garcia-Martinez E, Daviaud C, Kravak J, Aryankalayil J, Formenti SC, Demaria S. Radiotherapy cooperates with IL15 to induce antitumor immune responses. *Cancer Immunol Res.* 2020;8(8):1054–1063. doi:10.1158/2326-6066.CIR-19-0338.
  46. Creelan BC, Antonia SJ. The NKG2A immune checkpoint - a new direction in cancer immunotherapy. *Nat Rev Clin Oncol.* 2019;16(5):277–278. doi:10.1038/s41571-019-0182-8.
  47. Nishikado H, Mukai K, Kawano Y, Minegishi Y, Karasuyama H. NK cell-depleting anti-asialo GM1 antibody exhibits a lethal off-target effect on basophils in vivo. *J Immunol.* 2011;186(10):5766–5771. doi:10.4049/jimmunol.1100370.
  48. Assarsson E, Kambayashi T, Sandberg JK, Hong S, Taniguchi M, Van Kaer L, Ljunggren HG, Chambers BJ. CD8+T cells rapidly acquire NK1.1 and NK cell-associated molecules upon stimulation in vitro and in vivo. *J Immunol.* 2000;165(7):3673–3679. doi:10.4049/jimmunol.165.7.3673.
  49. De La Cruz-merino L, Chiesa M, Caballero R, Rojo F, Palazón N, Carrasco FH, Sánchez-Margalet V. Breast cancer immunology and immunotherapy: Current status and future perspectives. *Int Rev Cell Mol Biol.* 2017;331:1–53.
  50. Emens LA. Breast cancer immunotherapy: Facts and hopes. *Clin Cancer Res.* 2018;24(3):511–520. doi:10.1158/1078-0432.CCR-16-3001.
  51. Rugo HS, Delord JP, Im SA, Ott PA, Piha-Paul SA, Bedard PL, Sachdev J, Le Tourneau C, van Brummelen EMJ, Varga A, et al. Safety and antitumor activity of pembrolizumab in patients with estrogen receptor-positive/human epidermal growth factor receptor 2-negative advanced breast cancer. *Clin Cancer Res.* 2018;24(12):2804–2811. doi:10.1158/1078-0432.CCR-17-3452.
  52. Corrales L, Woo SR, Williams JB, McWhirter SM, Dubensky TW Jr., Gajewski TF. Antagonism of the STING pathway via activation of the AIM2 inflammasome by intracellular DNA. *J Immunol.* 2016;196(7):3191–3198. doi:10.4049/jimmunol.1502538.
  53. Swanson KV, Deng M, Ting JP. The NLRP3 inflammasome: molecular activation and regulation to therapeutics. *Nat Rev Immunol.* 2019;19(8):477–489. doi:10.1038/s41577-019-0165-0.
  54. Spicer JF, Marabelle A, Baurain JF, Awada A, Kristeleit RS, Jossang DE, Jebsen N, Loirat D, Armstrong AC, Curigliano G, et al. A phase I/II study of the oncolytic peptide LTX-315 combined with checkpoint inhibition generates de novo T-cell responses and clinical benefit in patients with advanced solid tumors. *J Clin Oncol.* 2018;36(15\_suppl):3094.